

# Polarizing-field orientation and thermal treatment effects on the dielectric behavior of fluorapatite

Aglaia Vassilikou-Dova<sup>a)</sup> and Ioannis M. Kalogeras

*Department of Physics, Solid State Physics Section, University of Athens, Panepistimiopolis, 157 84 Zografos, Greece*

Bogusław Macalik

*Polish Academy of Sciences, Institute of Low Temperature and Structure Research, 50-950 Wrocław, Poland*

Charalambos A. Londos

*Department of Physics, Solid State Physics Section, University of Athens, Panepistimiopolis, 157 84 Zografos, Greece*

(Received 13 May 1998; accepted for publication 6 October 1998)

A thermally stimulated depolarization currents (TSDC) study in natural fluorapatite single crystals has established different relaxation mechanisms for two polarization orientations ( $\mathbf{E}_p$  parallel and perpendicular to the crystallographic  $c$  axis), which are discussed in relation to the defect chemistry and the specific columnar structure in apatite. The intensities of the thermostimulated current signals between the two poling field orientations demonstrate a difference of at least one order of magnitude, with the higher one recorded for the electric field parallel to the  $c$  axis. The TSDC thermogram appearing with the electric field parallel to  $c$  axis, in the 10–320 K range, consists of a broad and complex band (HT), with a maximum around 300 K. The relative intensity of associated current signals is indicative of extensive dipole-like ionic motions along  $c$  axis with a distribution in their activation energies ranging between 0.14 and 0.85 eV. The microdomain structure of fluorapatite along  $c$  axis permits the formation of charge layers at the interfaces. After annealing, the induced changes of size and/or shape of the interfaces could explain the observed changes of band intensity and location. With the electric field perpendicular to  $c$  axis, the spectrum consists of at least five well-defined relaxation bands, the high temperature ones (HT<sub>1</sub>, HT<sub>2</sub>, HT<sub>3</sub>) decreasing after heating at 673–873 K. The most dramatic change was recorded for an intermediate LT<sub>2</sub> single-relaxation band located around 185 K, with a high activation energy of 1.06 eV, which manifested a significant growth after annealing. Rietvelt analysis of the x-ray diffraction patterns of the original and annealed apatite powders, indicates change in the unit cell parameters of the hexagonal structure (i.e.,  $a$  increases from 9.3921 to 9.3940 Å after annealing), which can be related to the establishment of a new equilibrium distribution of the abundant trivalent rare-earth (Ce, La, Nd, Pr,...) impurity ions. The origin of the TSDC bands is discussed and tentative correlations are suggested, in terms of substitute aliovalent ions-vacancy dipoles. The thermal response of the high temperature relaxation bands in the case of  $\mathbf{E}_p \perp c$  axis, is characteristic of dipole clustering phenomena—although an explanation based on localized changes in the structural environment of the pertinent dipoles/ions cannot be disregarded. © 1999 American Institute of Physics. [S0021-8979(99)10001-X]

## I. INTRODUCTION

The apatite group inherited its name (from the Greek “ $\alpha\pi\alpha\tau\acute{\alpha}\omega$ ” = *I delude*) prior to the end of the 18th century, through Werner’s recognition that its members were frequently confused with other mineral species. Apatite with the general chemical formula  $\text{Ca}_{10}(\text{PO}_4)_6(\text{F}, \text{OH}, \text{Cl})_2$  is a material found in nature and also synthetically prepared, with a high technological interest in material science.<sup>1–5</sup> The group members usually belong to the  $P6_3/m$  space group and their extremely stable structure allows many chemical modifications, as well as the incorporation of a wide number of impurities.<sup>6–9</sup>

The apatitic structure can be described briefly as follows (Fig. 1, Ref. 10).  $\text{PO}_4$  tetrahedra are arranged in trees around hexad axes (screw axes  $6_3$ ) forming columns parallel to the crystallographic  $c$  axis, with halogen and hydroxyl ions arranged along the column axis. The two distinguishing Ca structural locations have dissimilar stereochemistries. 6/10 of the  $\text{Ca}^{2+}$  ions per unit cell, occupying the so-called Ca(2) site, line the columns internally and tie in the  $\text{X}=(\text{F}^-, \text{OH}^-, \text{Cl}^-)$  ions in addition to holding the assemblage together. Each of them is one of the triad that surrounds and is coplanar with an  $\text{X}^-$  ion at each corner of the unit cell. Their coordination polyhedron is very irregular and approximates to coordination number VII, consisting of six O and one X anions ( $\text{CaO}_6\text{X}$ ). The remaining four  $\text{Ca}^{2+}$  ions, occupying the so-called Ca(1) sites, link neighboring

<sup>a)</sup>Corresponding author; electronic mail: avasilik@atlas.uoa.ariadne-t.gr

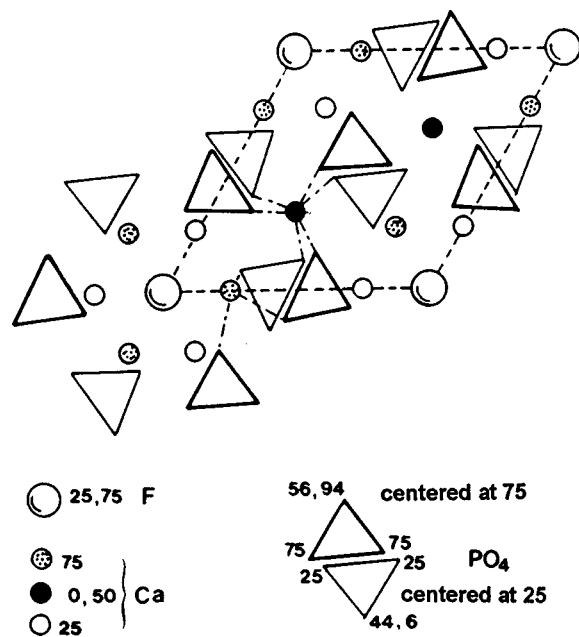


FIG. 1. Structure of fluorapatite projected on (0001) plane. Elevations are represented as percentages of  $c$ . Mirror planes are located at 0.25 and 0.75  $c$ .  $\text{Ca}^{2+}$  ions on 0, 50  $c$  occupy the Ca(1) lattice sites, while those at elevations 25, 75  $c$  correspond to the Ca(2) sites.

columns. Ca(1) sites have a coordination number IX ( $\text{CaO}_9$  polyhedron with average  $\text{Ca-O} = 2.554 \text{ \AA}$  in fluorapatite) in a regular trigonal antiprism with  $\bar{6}$  symmetry and are coplanar with three widely spaced  $\text{O}^{2-}$  ions that form a mirror plane bisecting a trigonal prism. The above atomic arrangement forms a hexagonal network. It should be pointed out that for fluorapatite, at least, the “tunnels” or “channels,” referred to by some authors<sup>11</sup> for describing the neighboring columns, are not a realistic model inasmuch as the Ca to F bond of the triangular configuration  $\text{FCa}_3$  on the  $6_3$  axis appears to involve distances that are slightly less than the sum of the radii for  $\text{F}^{\text{III}}$  and  $\text{Ca}^{\text{VII}}$ .

Apatite in various forms has been the subject for numerous studies involving the application of spectroscopic and electrical methods.<sup>8,12-14</sup> Its complicated structure and the multiplicity of substitutions offer a prominent background for the creation of vacancies, electrical dipoles or dipolar complexes, whose behavior is expected to be anisotropic. The thermally stimulated depolarization currents (TSDC) technique has been proved to be very sensitive for the characterization of fundamental temperature-dependent dipolar or dipolar-like motions,<sup>15</sup> which contribute to a change in the dielectric polarizability of the material along preselected orientations (e.g., direction of the polarizing field). Such characterization provides information about the atomic scale orientationally dependent relaxation mechanisms. The TSDC technique has been successfully applied in studies of fluorapatite (Fap, Ref. 16), chlorapatite (Cl-ap, Ref. 12), hydroxyapatite (OH-ap, Ref. 14), A-type carbonated apatite  $\{\text{Sr}_{10}(\text{AsO}_4)_6\text{CO}_3$ , Ref. 13}, and mixed apatitic structures.<sup>17</sup> Nevertheless, all direct current dielectric investigations, to the best of our knowledge, were performed with natural or synthetic apatitic material in compressed powder form, al-

though single crystal experiments could give valuable information based on the different behavior along different orientations. Earlier TSDC investigations have revealed compensation temperatures for the Cl-ap and OH-ap structures in agreement with the reported monoclinic-to-hexagonal phase transition temperatures.<sup>18</sup> At the other extreme lay the results collected for polycrystalline synthetic fluorapatites for which the analysis of the observed thermally activated processes in TSDC thermograms has not indicated any compensation phenomena below 1200 °C, that is, in agreement with reports stating that fluorapatite is structurally stabilized in this temperature range.<sup>17</sup> The present work reports on the results of the investigation of the effect of poling field orientation on the dielectric response of a natural fluorapatite single crystal from Cerro de Mercado, Durango, Mexico. Studies involving the magnetic properties of this mineral indicate that the magnetic susceptibility of the Durango fluorapatite is very low,<sup>19</sup> as would be expected because of the very low iron and manganese content. In two other cases,<sup>7,19</sup> the mineralogy and geochemistry, as well as the elastic properties, of fluorapatites from this locality have been extensively studied.

## II. EXPERIMENT

### A. The method

The TSDC method which was introduced by Bucci and Fieschi<sup>20</sup> has been widely established as a high resolution technique for the electrical characterization of dielectrics,<sup>21</sup> by virtue of its low detection limit of  $\sim 10^{-7}$  mole fraction of dipoles. The fundamental features of the typical experimental procedure can be summarized as follows:

(a) An external dc electric field is applied to the sample at a constant temperature  $T_p$  for a time period  $t_p$ , adequately chosen so that a saturation dipolar polarization can be reached [ $t_p \gg \tau(T_p)$ ]. The buildup of polarization  $P_0$  is described by the Langevin function and the relaxation time  $\tau(T)$  for dipole relaxation is usually defined according to the Arrhenius equation as

$$\tau(T) = \tau_0 \exp\left(\frac{E}{kT}\right). \quad (1)$$

(b) Keeping the field on, the sample is cooled down to a low temperature  $T_0$ , at which the relaxation time  $\tau(T_0)$  is very large compared to the time required for the experiment, resulting in a “frozen-in” polarization state. The field is removed and the sample remains short circuited at  $T_0$  for a time long enough so that the fast electronic and atomic polarization components can decay isothermally.

(c) The final step consists of a heating cycle at a preselected constant rate  $b = dT/dt$ . Each dipolar relaxation mechanism is activated within a certain temperature range at which the dipoles return to a random orientation. The rate of decrease of the corresponding dielectric polarization results to a transient current density  $J_D(T)$ , which reaches a maximum at a characteristic temperature  $T_m$ , fulfilling the condition

$$\left. \frac{d\tau}{dt} \right|_{T=T_m} = -1. \quad (2)$$

Under the description of the temperature-dependent properties of the Debye model, the resulting asymmetric current peak is described by the equation

$$J_D(T) = \frac{P_0}{\tau_0} \exp\left(-\frac{E}{kT}\right) \times \exp\left[-\frac{1}{b\tau_0} \int_{T_0}^T \exp\left(-\frac{E}{kT'}\right) dT'\right]. \quad (3)$$

The initial part of a single depolarization current peak (for current signals up to  $\sim 15\%$  of the maximum current intensity  $J_m$ ) is approximated by

$$J_D(T) = \frac{P_0}{\tau_0} \exp\left(-\frac{E}{kT}\right) \quad (4)$$

and thus the activation energy  $E$  can be calculated from the logarithmic plot of  $\ln J_D(T)$  vs  $T^{-1}$ . The relaxation time  $\tau(T)$  is calculated directly from the whole-curve graphical integration method.<sup>20</sup>

In systems with axial or lower symmetry, different relaxation mechanisms may appear along different axes and although the TSDC method provides no information about the symmetry of the dipolar system, comparison of the differentiation's encountered between the spectra with different polarization orientations can be valuable, as far as the dipolar-type defect chemistry is concerned. Moreover, the temperature-range overlap of more than one mechanism is not uncommon, and hidden relaxations of low intensity can arise after a suitable application of the external electric stimulus. In addition, cleaning procedures like the thermal sampling and partial discharge or depolarization techniques, as well as appropriate manipulation of the poling conditions ( $E_p, T_p, t_p$ ), can also lead to unraveling of complex relaxation spectra.<sup>22</sup>

## B. Experimental details

The subject matter in the present investigation were transparent, light yellow-greenish, fluorapatite crystals of gem quality from Cerro de Mercado, near Durango (Mexico), virtually free from inclusions and mineral coatings. The measuring samples were discs with thickness ranging between 1.0 and 1.4 mm, cut from a large prismatic crystal (approximately 3 1/4 cm long by 1 1/2 cm wide) in two perpendicular orientations, parallel and perpendicular to the crystallographic  $c$  axis, using the natural faces as a guide. A structural study of our sample was performed by measuring the x-ray diffraction (XRD) pattern ( $2\theta = 20^\circ - 90^\circ$ ), employing a Siemens D5000 powder diffractometer with Cu  $K\alpha$  radiation and a secondary monochromator at room temperature. A very good fit of the XRD powder patterns ( $R_{\text{Bragg}}$  factor 4.50%) was obtained via Rietveld analysis (program RIET<sup>23</sup>), based on a single phase hexagonal fluorapatite,  $a = 9.3921(2)$  Å,  $c = 6.8830(2)$  Å, with a space group  $P6_3/m$ . Table I contains the quantitative spectrographic analysis results, obtained by x-ray fluorescence

TABLE I. X-ray fluorescence (XRF) trace-element analysis of fluorapatite from Cerro de Mercado, Durango, Mexico.

Trace ions	Analysis in parts per million (ppm)
Substitution for $P^{5+}$	As <sup>5+</sup> 2668±90
Substitution for $Ca^{2+}$	Mn <sup>2+</sup> Nd. <sup>a</sup>
	Sr <sup>2+</sup> 497±15
	Y <sup>3+</sup> 823±24
	La <sup>3+</sup> 2398±218
	Ce <sup>3+</sup> 2736±288
	Pr <sup>3+</sup> 319±32
	Nd <sup>3+</sup> 990±100
	Sm <sup>3+</sup> 134±13
	Gd <sup>3+</sup> 99±10
	Th <sup>3+</sup> 418±21
	U <sup>3+</sup> 15.3±1.5

<sup>a</sup>Nd.—not determined by XRF analysis, but detected through the Mn<sup>2+</sup> ( $S = 5/2, I = 3/2$ ) sextets appearing in the EPR spectra of the Durango fluorapatite.

(XRF), for Fap crystals. Several other light substitute ions (like, Si<sup>4+</sup>, Na<sup>+</sup>, K<sup>+</sup>, and Cl<sup>-</sup>), are also expected to enrich the fluorapatitic structure. However, their concentration cannot be determined by XRF analysis. In a particular case, the presence of paramagnetic Mn<sup>2+</sup> ions ( $S = 5/2, I = 5/2$ ), of unknown concentration (possibly  $< 10$  ppm), has been verified by a complementary electron paramagnetic resonance (EPR) study.

The TSDC scans were carried out in a Leybold–Heraus ROC 10–300 refrigerator-cooled cryostat, accordingly modified for electrical measurements. The R210 two-stage refrigerator used to operate the cryostat is a cryogenerator operating the Gifford–McMahon principle, utilizing the provided closed helium-gas cycle by a suitable compressor unit (model RW2). The experiment was performed under vacuum conditions ( $\cong 10^{-4} - 10^{-5}$  Torr) with the use of a Drytel pump. The dc electric field was applied along the two orientations ( $\mathbf{E}_p \parallel c$  and  $\mathbf{E}_p \perp c$ ), between stainless-steel electrodes electrolytically covered by chromium. The computer controlled measurements were carried out in the temperature range of 10–320 K with the typical experimental conditions of  $T_p = 320$  K,  $E_p = 18$  kV/cm, and  $t_p = 5$  min, for which a saturation polarization is reached. The typical cooling and heating rates were  $(5.0 \pm 0.2)$  deg/min and temperature regulation was achieved using a digital LTC 60 microprocessor controlled unit (Leybold–Heraus). Thermocurrent signals were monitored by a Keithley 617 programmable electrometer. Annealing in all samples was performed in air for one hour at three different temperatures (673, 773, and 873 K), followed by quenching at RT at a rate exceeding 100°/min.

## III. RESULTS

We shall classify our thermally stimulated depolarization currents results in two groups, in connection with the relative orientations of the applied electric field vector ( $\mathbf{E}_p$ ) and the crystallographic  $c$  axis.

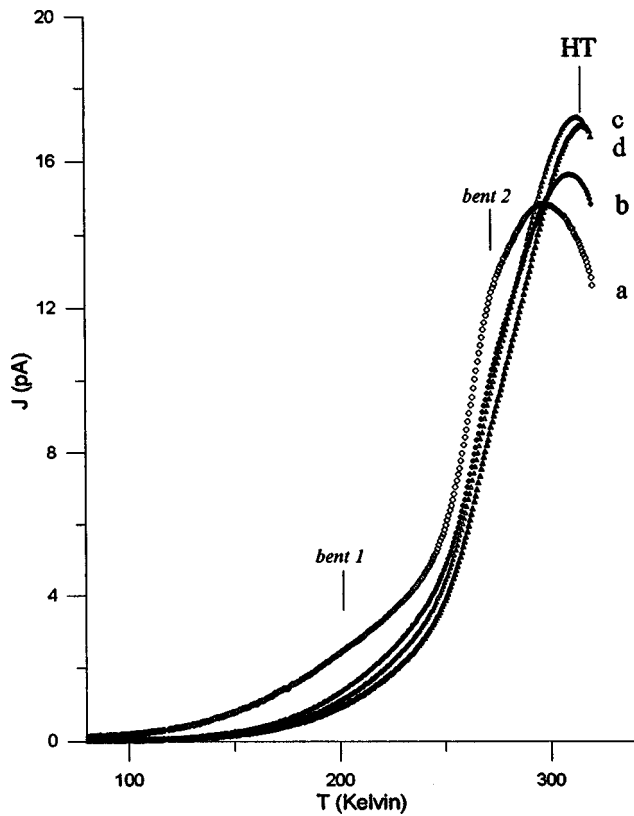


FIG. 2. Thermally stimulated depolarization current spectra for (a) thermally untreated and annealed samples at (b) 673 K, (c) 773 K, and (d) 873 K, polarized with  $E_p \parallel c$  axis.

**A. TSDC study with  $E_p$  parallel to  $c$  axis**

Typical TSDC spectra recorded for the as-received (A1) and thermally treated (B1) samples are depicted in Fig. 2 (curves a–d). The spectra are dominated by an intense broad band (denoted HT) which reaches a maximum around 300 K and extends almost throughout the entire temperature range under investigation.

The application of the polarization field  $E_p$  at different polarization temperatures  $T_p$ , within the 210–320 K temperature window, in both the A1 (presented in Fig. 3) and the B1 samples, manifested a strong dependence between  $T_p$  and the maximization temperature  $T_m$  ( $T_p$  lagging behind  $T_m$  by  $\sim 5^\circ$ – $15^\circ$ , with reversed behavior for  $T_p \geq 290$  K). This shift of  $T_m$  was also accompanied by an increase of the maximum current intensity  $J_m$  with increasing temperature of polarization. The HT thermocurrents' region of the A1 samples is apparently a complex relaxation band as two barely discernible knees appear in the TSDC spectrum at about 200 and 270 K, respectively.

Successive annealing of the B1 sample (at  $T = 673, 773,$  and  $873$  K, respectively) resulted in a  $10^\circ$ – $20^\circ$  shift of the main HT peak maximum to a higher temperature region accompanied by a moderate increase of  $J_m$ . Moreover, the rising part of the band (previously featuring a knee at 200 K) was progressively smoothed out without further changes in the appearance of the HT relaxation band (Fig. 2, curves b–d). The above observations, in connection with certain characteristics of the TSDC high temperature peak (e.g., not

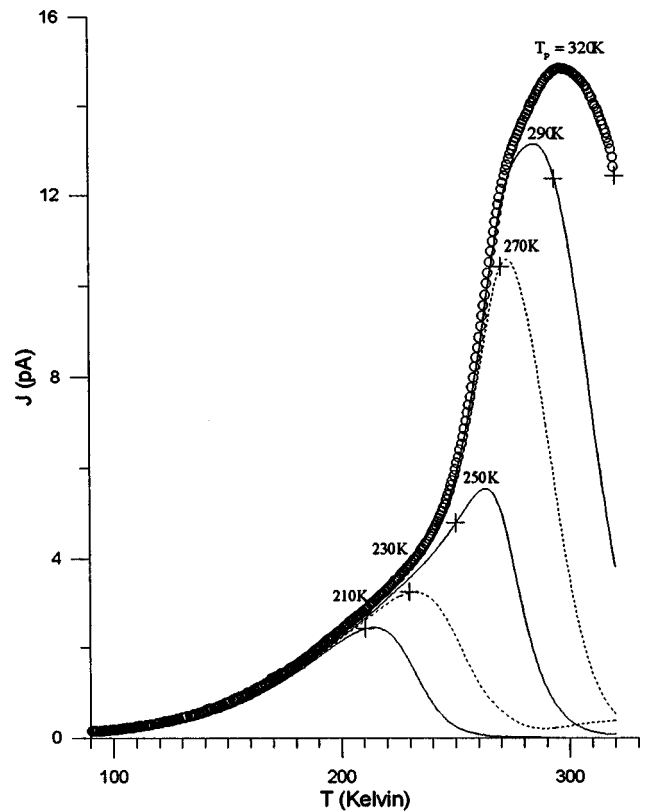


FIG. 3. Demonstrating the changes observed in the maximum of the TSDC curves of the untreated sample for variable polarization temperatures ( $T_p$ ) and  $E_p \parallel c$  axis. Crosses (+) indicate the position of  $T_p$  at each TSDC experimental run.

exponential rise, coverage of an extended temperature range) are a first indication of highly overlapped dielectric polarization mechanisms, presenting a spectrum of relaxation times  $\tau(T)$ . In order to decompose the band and obtain the energy spectrum of the relaxation mechanisms involved, we applied the partial discharge method (otherwise referred to as partial heating or partial depolarization method) in both specimens (A1 and B1) and at intervals of approximately  $10^\circ$  to cover the entire temperature range of interest (110–320 K). The analysis of the intensity current recordings by means of Eq. (4) yielded activation energy values ranging between 0.15 and 0.85 eV. Although there is no clear evidence for some stepwise changes in the plot of activation energy  $E$  vs the middle point of the discharge temperature range of each cycle  $T_{mp}$  (Fig. 4), within the experimental errors, there appears to be an accumulation of the energy parameters in the narrow spectral range  $(210 \pm 20)$  K at the values of  $(0.53 \pm 0.03)$  eV, for the original specimen, and  $(0.62 \pm 0.02)$  eV for the annealed sample, respectively.

**B. TSDC study with  $E_p$  perpendicular to  $c$  axis**

The TSDC spectrum of a thermally untreated (A2) sample with the electric field vector perpendicular to the crystallographic  $c$  axis is dominated by four overlapping bands that peak at approximately 172 K (denoted as  $LT_1$ ), 206 K ( $HT_1$ ), 235 K ( $HT_2$ ), and 316 K ( $HT_3$ ) (Fig. 5, curve a). We should note at this point the presence in the rising part of the  $HT_1$  band of a fifth, much narrower and extremely

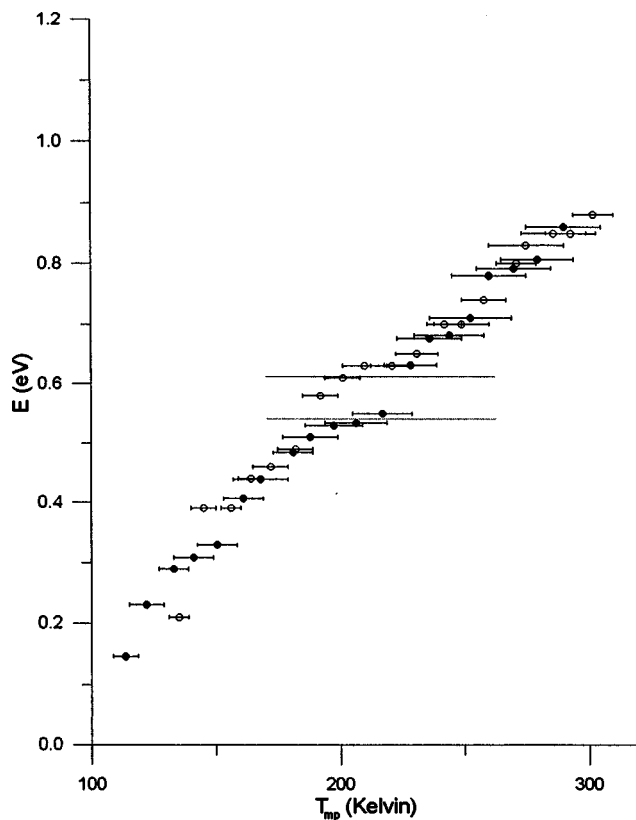


FIG. 4. Plot of the activation energies  $E$  vs the middle-point temperature of the partial discharge cycles  $T_{mp}$  for  $E_p \parallel c$  axis (● thermally untreated sample; ○: annealed at 773 K). Dashed lines are to guide the eye.

weak, current signal, peaking at about  $T_m = 183$  K [LT<sub>2</sub>, Fig. 5(a)] which in independent TSDC experiments showed high reproducibility.

The TSDC thermogram recorded after annealing the fluorapatite sample at 673 K (Fig. 5, curve b) for one hour, with subsequent quenching at room temperature, demonstrate a considerable reduction of the high temperature (HT<sub>1-3</sub>) peaks which progressively tend to disappear for higher annealing temperatures (773, 873 K). Especially in the case of the HT<sub>1</sub> relaxation band, in the course of the consecutive annealing procedures there was no substantial shift of its intensity maxima (Fig. 6, curves a–c). However, the most striking result after annealing is the manifestation of an intense and extremely sharp peak in the thermally treated (B2) sample, in the position where the weak LT<sub>2</sub> spike appeared in the spectrum of the as received sample [Fig. 5(a)]. The intensity maximum of this sharp peak appears to have reached its highest value after annealing at 773 K for one hour (Fig. 6, curve b), with a moderate reduction at the topmost annealing temperature (Fig. 6, curve c). By repeating the TSDC measurement with identical poling conditions one year following annealing, the entire spectrum and especially peak LT<sub>2</sub> does not show any considerable changes. Application of the electric field at different polarization temperatures  $T_p$  and times  $t_p$  leaves the peak characteristics ( $T_m$  and/or  $J_m$ ) unaffected for the three low temperature bands (LT<sub>1</sub>, LT<sub>2</sub>, and HT<sub>1</sub>), while the maximization temperature for HT<sub>3</sub> always lags behind  $T_p$ . Moreover, the current intensity

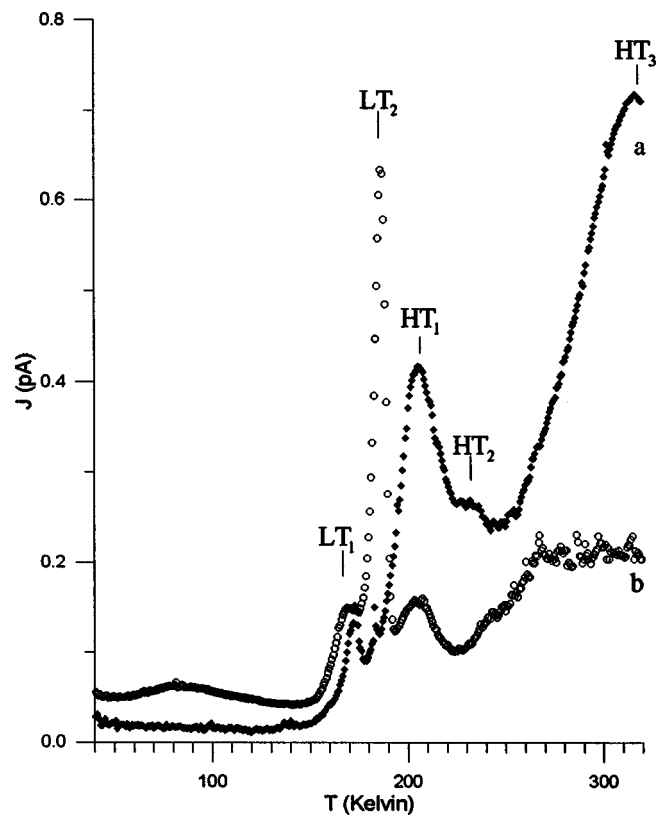


FIG. 5. Thermally stimulated depolarization current spectra for (a) thermally untreated and (b) annealed samples at 673 K, polarized with  $E_p \perp c$  axis, representative of the dramatic changes occurring in the low and high temperature spectral regions. Five clearly discernible relaxation bands are indicated.

maxima of the low temperature bands (LT<sub>1</sub> and LT<sub>2</sub>) show a linear dependence upon  $E_p$ .

For comparison purposes, we present in Fig. 7 a detailed scan of the TSDC spectrum of the as-received and annealed fluorapatite specimen, polarized with  $E_p$  parallel to the crystallographic  $c$  axis, in the temperature range of the LT<sub>1</sub> and LT<sub>2</sub> relaxations. From a direct comparison there appears to be no evidence about any similar relaxation signal, although we cannot firmly say the same for bands HT<sub>1</sub> and HT<sub>2</sub> which could be hidden below the left wing of the broad and intense HT relaxation band depicted in Fig. 2.

Analysis of the consecutive current rises collected by means of the partial heating method, applied in intervals of approximately 10° between 110 and 320 K for the A2 and B2 samples, gave results which are presented in Fig. 8. The straight line fitting of the points of the Arrhenius plot for the lower part of the complex spectrum, which coincides with the rising left wing of LT<sub>1</sub> peak, presents a (re)orientation activation energy of  $E_1 = (0.38 \pm 0.02)$  eV. A little higher, in the temperature range where LT<sub>2</sub> peak appears, there is a sudden sharp increase in the calculated activation energy values which reach a maximum at  $E_2^A = (0.86 \pm 0.03)$  eV in the as-received sample and  $E_2^B = (1.06 \pm 0.01)$  eV in the thermally treated sample. In the region of the HT<sub>1</sub> and HT<sub>2</sub> bands, around 200–240 K, the evaluation of the data for both samples gave activation energies between  $E_3 = (0.60 - 0.70)$  eV. The dominating HT<sub>3</sub> band in the latter part of the

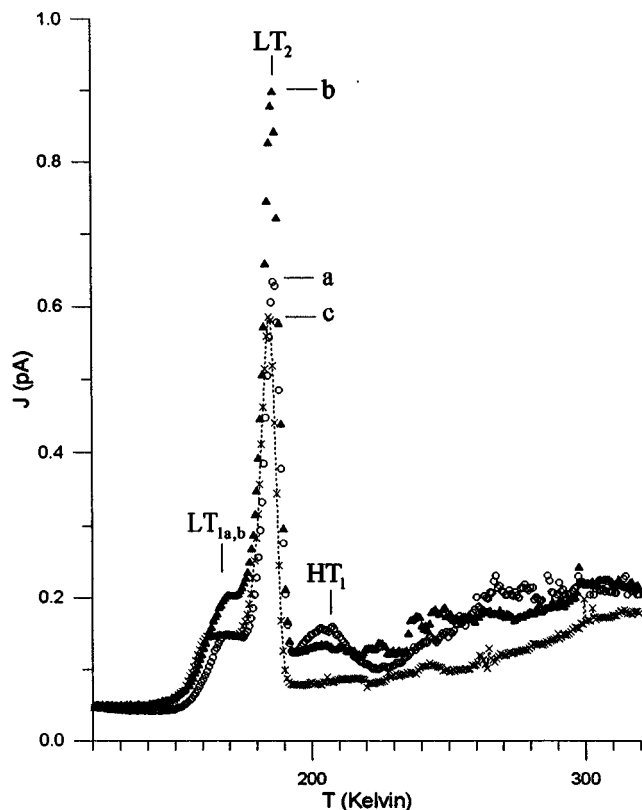


FIG. 6. Comparative TSDC spectra for thermally treated samples at (a) 673 K, (b) 773 K, and (c) 873 K, polarized with  $E_p \perp c$  axis. The most interesting effect is the gradual decrease of the high temperature relaxation bands.

A2 thermogram demonstrates energy values  $E_4$  around 0.82 eV.

#### IV. DISCUSSION

The dielectric relaxation of an insulator is due to the rotation of impurity-vacancy ( $I-V$ ) dipoles or molecules with intrinsic polarity, as well as to a migration process of a limited number of free electric charge carriers (e.g., electrons and ions). When aliovalent impurities are incorporated into a solid matrix, for charge compensation reasons an appreciable number of vacancies are formed. Such cation vacancies, when bound to a substitution impurity ion, form different kinds of  $I-V$  dipoles, with dependence on the relative charge distance, and under certain conditions, they can constitute larger polar complexes.<sup>24,25</sup> Moreover, the existence of free vacancies as free charge carriers is not uncommon in ionic crystals, and their drift in-between structural openings customarily dominates the high temperature (in the TSDC measurements) or low frequency (normally below 1 Hz in the ac dielectric spectroscopy) relaxation domains.

It is a well-established fact that the close packing and nonpolymerized nature of the  $[\text{PO}_4]$  groups in the unperturbed apatitic lattice inhibits the concentration of selective polarizability along axial or preferred directions. However, the preconditions for the development of macroscopic dielectric polarizability and charge storage at low temperatures are fulfilled if one takes into account in detail the apatite's crystal structure data. The large dielectric effects previously ob-

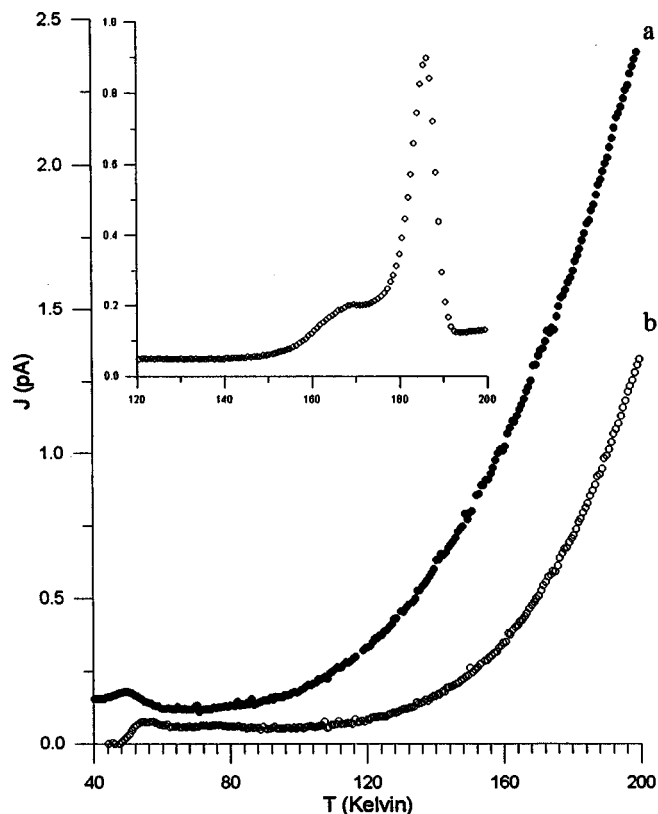


FIG. 7. Detailed scan of the low temperature range for (a) thermally untreated and (b) annealed samples at 673 K, polarized with  $E_p \parallel c$  axis. The LT range clearly lacks of thermocurrent signals that can be related to the mechanisms observed in the annealed spectrum for  $E_p \perp c$  axis (inset).

served in monoclinic (space group  $P2_1/b$ ) synthetic chlorapatites  $[\text{Ca}_{10}(\text{PO}_4)_6\text{Cl}_2]$  studied by ac dielectric relaxation spectroscopy methods,<sup>12</sup> despite their x-ray characterization as nonpolar crystal structures, are accounted for by a  $\text{Cl}^-$ -vacancy driven relaxation mechanism.<sup>26</sup> The creation of  $\text{Cl}^-$  vacancies provides space in the apatitic columns necessary to allow the chlorine ions (at heights  $z \approx 0, 1/2c$  in the monoclinic cell) to move individually. Chlorapatites with 5%  $\text{Cl}^-$  vacancies were reported to exhibit dielectric permittivities ( $\epsilon'$ ) exceeding  $10^4$  when the vector of the electric stimulus was parallel to the crystallographic  $c$  axis.<sup>26</sup> The presence of vacancies in the contacting  $\text{Cl}^-$ - $\text{Cl}^-$  ions along the columns is somewhat dictated by the fact that the ordinary  $\text{Cl}^-$  ionic radii (1.81 Å) exceed by 0.24 Å the  $\text{Cl}^-$ - $\text{Cl}^-$  distance ( $\sim 3.38$  Å), and as a result individual Cl ions tend to be displaced towards the adjacent chlorine anion-vacancies. The intrinsic electric dipole in the chlorapatitic structure arises from the displacement of chlorine from the ideal symmetry position (at  $z=0, 1/2c$  in the monoclinic cell), as the  $\text{Cl}^-$  ions occur at  $z$  positions distant  $\delta$  from the midpoints between the Ca(2)-triangles (perpendicular to the columns at  $z=1/4, 3/4c$ ). The resulting  $\text{Cl}^-$ -Ca(2)<sup>2+</sup> configuration constitutes a dipolar structure in which the electric dipole direction can be reversed by the mere movement of the  $\text{Cl}^-$  ion from  $z=1/2+\delta$  to  $z=1/2-\delta$ .

In fluorapatite, the  $6_3$  axis of  $\text{F}^-$  ions (at  $z=1/4, 3/4c$  in the hexagonal cell) passes perpendicularly to the planes of the adjacent Ca(2) triangles and through their centers. In its

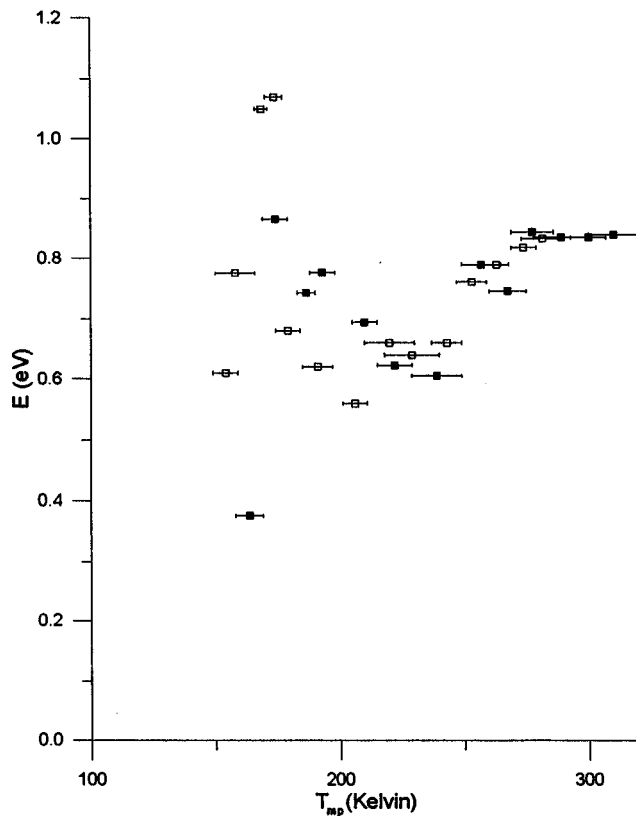


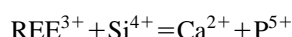
FIG. 8. Plot of the activation energies  $E$  vs the middle-point temperature of the partial discharge cycles  $T_{mp}$  for  $E_p \perp c$  axis (■: thermally untreated sample; □: annealed at 773 K).

pure stoichiometric form, the  $F^-$  ion exists exactly at the center of the calcium triangle and experiences no electrostatic forces tending to move it away [Ca-(O, F) distance of approximately 2.463 Å]. Such a configuration of the mineral structure does not allow the formation of dipole units and would normally render inapplicable dielectric methods in pure Fap crystals. This is not the case in fluorapatites that are compositionally modified. In fluorhydroxyapatite [ $Ca_{10}(PO_4)_6(F, OH)_2$ ] for instance, the  $F^-$  may have  $OH^-$  neighbors, and hydrogen bonding (F...H-O) could cause fluorine to move slightly out of the plane of the calcium triangle.<sup>27</sup> Even in the absence of  $OH^-$  ions, both Ca sites in Fap are able to accommodate a variety of aliovalent (univalent, divalent and/or trivalent) cations. Among the transition metal ions we site manganese which can partially replace calcium<sup>8</sup> in a not uncommon  $Mn^{2+}/Ca^{2+}$  maximum ratio of approximately 1:10.<sup>1</sup> Nevertheless, the most common group of substitutes constitute the rare-earth elements La to Lu (REE). These transition metals, with a progressive filling of the 4*f* electron shell, are common minor or trace constituents in Ca structural positions of rock-forming minerals of all geological environments.<sup>28-30</sup> The progressive decrease in ionic radius through the lanthanides series (with increasing atomic number) arises from imperfect shielding of one 4*f* electron by another 4*f* electron, and their crystal chemistry is dominated by simple space fitting requirements. Although the bond valence requirement is probably the most important factor controlling REE site occupancy in apatite, the selec-

tivity of apatite in individual REE appears to be dominated by spatial accommodation alone. In the case of the Durango fluorapatites, high concentrations in light REE (LREE, predominantly La and Ce), as well as in  $Sr^{4+}$ , have been verified by independent investigators<sup>6,7,31</sup> and the present XRF trace-elements analysis.

In the present study, the TSDC spectra of Fap single crystals and the quantitative analysis of the data give information about the relaxation parameters of the dielectrically active relaxation modes in the apatite structure. The evaluation of the corresponding thermodynamic parameters, give evidence that the ordering/disordering information is propagated differently along two perpendicular directions (parallel and perpendicular to the crystallographic *c*-axis), following different relaxation mechanisms. A difference of 25% between the values of the radiofrequencies dielectric permittivity of apatite from Asio (Japan) for the two orientations ( $\epsilon' = 10.0$  for  $E_p \parallel c$  and 7.6 when  $E_p \perp c$ ) supports this statement.<sup>32</sup> An  $F^-$  (or  $Cl^-$ )-vacancy translational relaxation mechanism along the columns on the 6<sub>3</sub> screw axis can be used to describe the presence of the strong thermocurrent signals appearing in the TSDC spectra recorded for fluorapatite when the electric vector was parallel to the crystallographic *c* axis (HT band in the as-received A1 and B1 fluorapatite samples). Therefore, the main mechanism along *c* direction seems to be governed by dipolar reorientation induced by the jumps of the  $F^-$  (and/or  $Cl^-$ ) ions located in the apatite columns. The existence of an increasing trend of the (re)orientational activation energies with scanning temperature can be therefore connected with the presence of a distribution of microdomains in space along the *c* axis where the environment of a halogen-vacancy passes through more or less dramatic changes. The above distribution pattern is most likely joined by contributions of strongly overlapping secondary relaxation mechanisms. Earlier studies by Phakey and Leonard attribute the long prismatic habit of natural apatites to "pure screw dislocations which align with the *c* axis, and mixed dislocations which deviate slightly from alignment with the *c* axis."<sup>33</sup> The distortion in the interionic distances at microdomains induced by the various dislocations provide easy paths for short range cation/anion migration (limited within a few interatomic distances), especially by virtue of their relative aligning with the crystallographic *c* axis. Such structural imperfections are perfect alternative candidates for the appearance of the enhanced ionic and space charge mobility in the TSDC experiments of this poling configuration. The resulting difference between the electrical conductivity and dielectric permittivity of imperfections and matrix, forms the basis for the creation of a MWS interfacial polarization. In the fluorapatites case, the dislocation lines surrounded by impurities play the role of inhomogeneities, with the formation of charge layers at the interface between imperfections and the "good" lattice. Thus, especially in the high temperature part of the HT band, it is expected to record a MWS polarization contribution. After annealing the observed changes of band intensity and location can be related with changing of size and/or shape of existing imperfections or the creation of a new one.

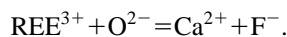
In relation to the second category of experiments ( $E_p \perp c$ ) great attention has to be paid in polarization modes associated with the creation and selective partitioning of several structural defects. In an extended study in natural and synthetic fluorapatites by Fleet and Pan<sup>6</sup> and the large body of references cited therein, the predictions of REE site preference and selectivity of the host mineral are conclusive to the proposal that light lanthanides (La, Ce, Pr, Nd) preferentially partition into fluorapatite and in particular favor the underbonded position Ca(2). The above hypothesis is supported by our XRF trace-element analysis of the Cerro de Mercado fluorapatite samples (Table I), which also indicates an appreciable amount of  $\text{Sr}^{2+}$ ,  $\text{Y}^{3+}$  in addition to the actinides series elements of thorium and uranium (i.e., 418 ppm  $\text{Th}^{3+}$  and 15.3 ppm  $\text{U}^{3+}$ ). The LREE substitution for calcium in the Ca(2) positions, with the lower coordination number, accordingly increases the bond valences of these positions. Moreover, the total stereochemistry of the Ca(2), and to a lower degree Ca(1), positions occupied by  $\text{REE}^{3+}$  is clearly modified. The substitution of  $\text{REE}^{3+}$  into apatite may be charge balanced in various ways (e.g., see Ref. 34) although a common way appears to be



or



The fact that for the rare-earth elements, the valence state is higher than that of the host ion, implies the necessity of a higher (than the thermodynamically induced) number of cation vacancies<sup>3</sup> and/or anion substitution. As an alternative, many authors assume that the excess of positive charge in the apatitic lattice can also be compensated by the substitution of oxygen for fluorine<sup>35</sup>



Limited  $\text{Cl}^- \rightarrow \text{F}^-$  substitution in the natural hexagonal skeleton of Durango Fap (e.g., Young *et al.* report a fluorine/chlorine weight percent ratio of 3.54:0.41, Ref. 19) leads to a chlorine shift readily explained by the much larger radius of  $\text{Cl}^-$  compared with  $\text{F}^-$ , and followed by a moderate change in bond lengths. The fluorapatite crystals employed in the present investigation demonstrate lattice constants  $a = 9.3921 \text{ \AA}$  and  $c = 6.8830 \text{ \AA}$ , which are similar to former reports for apatites from the same locality (9.3923  $\text{ \AA}$ , 6.8821  $\text{ \AA}$ , Ref. 19) and clearly distinguished from the lattice constants for pure Fap crystals (9.367, 6.884  $\text{ \AA}$ ). The main source of the observed variation in the unit cell parameters are the  $\text{REE}^{3+} \rightarrow \text{Ca}^{2+}$ ,  $\text{As}^{5+} \rightarrow \text{P}^{5+}$  ( $r_{\text{As}}^{(\text{IX})} \geq r_{\text{P}}^{(\text{IX})} + 0.11 \text{ \AA}$ ) and  $\text{F}^- \leftrightarrow \text{Cl}^-/\text{OH}^-$  substitutions. As a result, the  $\text{PO}_4$  tetrahedra are significantly distorted, being elongated along the P-O(2) direction, to a degree very similar to the Cl-ap and OH-ap structures.<sup>9,36</sup>

A theoretical interpretation of the experimental data in the sense of making attribution of the relaxation spectra, in response to the electric poling field in the crystallographic  $c$ -axis direction, to definite microstructural mechanisms is difficult to be done. However, in the light of the foregoing discussion the following assignment could be put forward. A

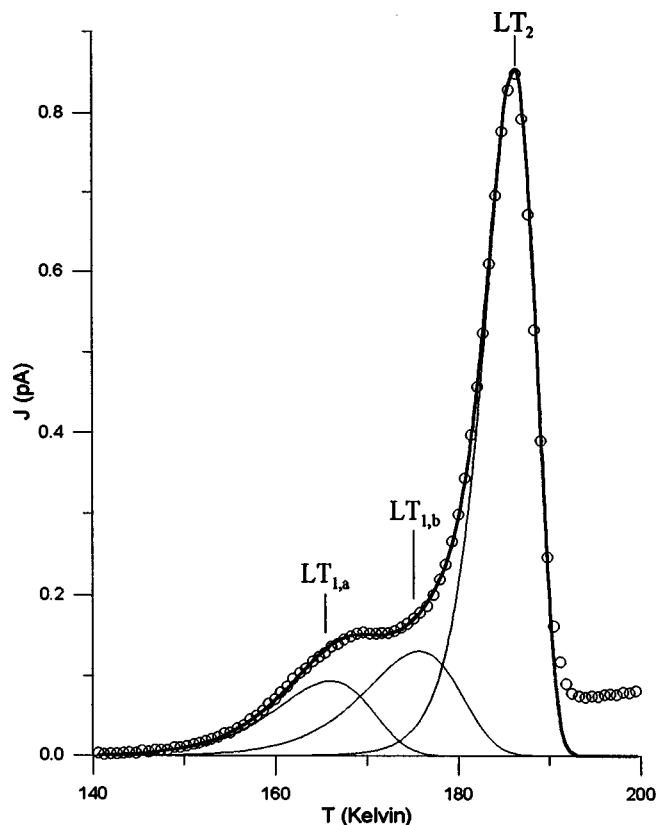


FIG. 9. Elementary peaks ( $\text{LT}_{1a}$ ,  $\text{LT}_{1b}$ ) composing the lowest temperature relaxation band ( $\text{LT}_1$ ) of the  $E_p \perp c$  axis TSDC spectra, shown here for annealing temperature 773 K. The  $\text{LT}_{1a,b}$  and  $\text{LT}_2$  monoenergetic peaks resolved by the fitting procedure show an envelope (thick line) accurate reproduction of the experimental points (open circles).

curve fitting method analysis of the low temperature current signals in both the A2 and B2 spectra (e.g., Fig. 9 for the B2 sample) has revealed that the  $\text{LT}_1$  band is due to the coalescence of two highly overlapped relaxations (denoted  $\text{LT}_{1a}$ ,  $\text{LT}_{1b}$ ). Both, the dipolar-type compatible response recorded between different TSDC experiments, and the range of the activation energies associated with the corresponding molecular mechanism responsible for the complex  $\text{LT}_1$  band (Table II), advocate a dipolar interpretation of either one of the following polarizability modes: (a) electric dipoles formed by chlorine/fluorine ions which are vertically or horizontally displaced from their ideal symmetry position at the columns, due to electrostatic forces by the trivalent rare earth ions residing on Ca(2) and nearby cation sites, and the positive charge of the Ca(2) triangles, and (b) cation jumping forth and back, on the ( $ab$ ) plane, between two of the nearest neighbor (nn) positions of a cation vacancy. As regards the second relaxation mode, it seems rational to hypothesize that the neighboring relaxations could arise from aliovalent substitute cations. In that case the low temperature peak ( $\text{LT}_{1a}$ ; Fig. 9) is assigned to the  $\text{Na}^+$  substitute ions, characterized by the smaller ionic radius comparable to calcium (for VII and IX coordination  $r_{\text{Na}} = r_{\text{Ca}} - 0.02 \text{ \AA}$ ), and the higher temperature peak ( $\text{LT}_{1b}$ ; Fig. 9) to the larger LREE<sup>3+</sup> ions (ionic radii typically  $r_{\text{REE}}^{(\text{VII,IX})} \geq r_{\text{Ca}}^{(\text{VII,IX})} + 0.05 \text{ \AA}$ ).

By virtue of the present results, the changes observed in the entire temperature range of the thermocurrents spectrum

TABLE II. Thermodynamic and spectral parameters for the fluorapatite sample polarized perpendicular to  $c$  axis ( $\vec{E}_p \perp c$ ). A2 denotes the as-received sample and B2 the sample annealed at 773 K for one hour.

Band	$T_m$ (K)		$J_m^r (\times 10^{-4} \text{ s}^{-1})^a$		$E$ (eV)	
	A2	B2	A2	B2	A2	B2
LT <sub>1a</sub>	(160) <sup>b</sup>	(166)			0.38 ± 0.02 (0.60)	0.62 ± 0.02 (0.44)
LT <sub>1b</sub>	(172)	(176)			(0.66)	(0.50)
LT <sub>2</sub>	183	186	~1.9	14.43	0.86 ± 0.03	1.06 ± 0.01 <sup>c</sup>
HT <sub>1</sub>	206	205	5.67	1.5	0.70 ± 0.10	...
HT <sub>2</sub>	235	uncertain	3.55	~1.5	0.62 ± 0.02	0.66 ± 0.03
HT <sub>3</sub>	314	uncertain	9.86	~2.9	0.82 ± 0.02	...

<sup>a</sup> $J_m^r$  represents the current density value at the position of the maximum, corrected for the sample dimensions (surface area  $S$  and thickness  $d$ ) and the polarizing field strength, through the relation  $J_m^r = J_m / \epsilon_0 S E_p$ , where  $\epsilon_0 = 8.85419 \times 10^{-12}$  Cb/m V.

<sup>b</sup>The values given in brackets were obtained from the curve fitting of the spectral LT<sub>1</sub> complex band. All other  $T_m$  and  $J_m^r$  values are spectral parameters.

<sup>c</sup>Both the fitting value and the energy value inferred by means of the partial heating method coincide. The pre-exponential factor of the Arrhenius Eq. (1) for the single LT<sub>2</sub> band is calculated to be  $\tau_0 = 6.04 \times 10^{-28}$  s.

after heating are associated with localized changes in the equilibrium ionic distribution, initiated by the temperature enhanced amplitude of the lattice vibrations as a whole, and the thermal energy of the ions which is sufficient for surpassing high potential wells after annealing at elevated temperature ranges. The XRD data analysis supports the above hypothesis, since there appear strong differentiation in lattice constants and to a lower degree in several bond distances (Table III). The most pronounced change has been calculated for the ( $a, b$ ) dimension, while small differences in excess of the calculation error, appear for the Ca(2)–O(2) and P–O(2) bond distances. The LT<sub>2</sub> peak, in particular, barely appears in the A2 orientation spectrum, implying a very low concentration ( $N_D$ ) of related dipole units (peak's area is proportional to  $N_D \mu^2$ , where  $\mu$  is the effective dipole moment). After annealing the LT<sub>2</sub> peak becomes the predominant signal with a high single activation energy (1.06 eV) and extremely low pre-exponential factor  $\tau_0$  ( $\sim 10^{-28}$  s), unusual for thermostimulated current dielectric studies. Under the new energetic/ionic conditions which develop in the sur-

rounding area of some ionic positions, in the “quenched” apatite structure after annealing, pre-existing mechanisms may become energetically unfavorable or simply frozen up due to simple steric hindrance. On the other hand, new ion jumping relaxation bands may appear, by simply considering the presence of new types of vacant structural sites. The appearance of the LT<sub>2</sub> relaxation peak even one year after the heating procedures and with the sample stored at RT conditions, indicates that the microstructural configuration developed after annealing is, at least, partially retained. The above observations favor an explanation based on a polarizability mode, involving ions jumping between vacant next-nearest-neighbor (nnn) positions that are located outside the columnar regions. We should also take into account that the heating procedure has been performed in oxygen atmosphere, which is a known element for its reactive properties, although by performing standard differential thermal analysis (DTA) of a Fap sample we did not find any evidence of weight change in the temperature ranges of interest.

In ionic crystals and minerals, the phenomenon of a sub-

TABLE III. Lattice parameters and bond distances obtained by Rietvelt analysis of the x-ray diffraction powder patterns of fluoapatite from Cerro de Mercado (Mexico), before and after annealing (at 773 K for one hour).

	As-received sample			Annealed sample			
Cell parameters (Å)	$a$	9.3921 (2)		9.3940 (2)			
	$c$	6.8830 (2)		6.8822 (2)			
Site		Ca(1)	Ca(2)	P	Ca(1)	Ca(2)	P
Fractional coordinates	$x$	1/3	0.2418 (2)	0.3997 (3)	1/3	0.2420 (3)	0.3993 (4)
	$y$	2/3	0.9920 (3)	0.3705 (3)	2/3	0.9914 (3)	0.3691 (4)
	$z$	0.0029 (5)	1/4	1/4	0.0037 (6)	1/4	1/4
	$B$	0.801	0.846	0.632	0.801	0.846	0.632
Bond distances (Å)	O(1)	2.365 (5)	2.688 (6)	1.571 (8)	2.361 (4)	2.682 (7)	1.583 (9)
	O(2)	2.470 (6)	2.335 (6)	1.570 (5)	2.475 (7)	2.356 (7)	1.547 (6)
	O(3)	2.818 (3)	2.348 (4)	1.536 (4)	2.819 (6)	2.336 (4)	1.535 (4)
			2.508 (5)			2.525 (3)	
	$F$	...	2.310 (2)	...	...	2.315 (5)	...
$R_{wp}$		11.13			10.44		
$R_{exp}$		7.46			7.58		
$R_{Bragg}$		4.50			4.29		

stantial decrease in a TSDC relaxation band after annealing, when not apparently related to intercrystalline water adsorption or protonic conductivity effects, is usually attributed to clustering phenomena.<sup>24</sup> A process referring to dipole cluster formations whose concentration diminishes after annealing could explain the changes occurring at the HT relaxations appearing in the spectra where the  $\mathbf{E}_p \perp c$  configuration was used. Nonetheless, a simple clustering scheme is not supported by the observation that even one year after annealing the high temperature bands have not restored much of their magnitude, as would be normally expected by the kinetics of clustering processes.

## V. CONCLUSIONS

The TSDC technique has been applied to study the dielectric properties of fluorapatite single crystals for two poling field orientations, namely, parallel and perpendicular to the crystallographic  $c$  axis. The main depolarization current mechanisms along  $c$  axis are governed by dipolar reorientations in the apatite columns, through F and Cl jumps, and ionic motions at regions of long range structural defects (screw dislocations parallel to  $c$  axis). The almost linear dependence of the (re)orientation energies with scanning temperature can be attributed to a distribution of microdomains along the  $c$  axis, which differentiate the ionic surroundings. The five distinct TSDC relaxations characterizing the spectra when the poling field was perpendicular to  $c$  axis are tentatively discussed, in order of appearing temperature range, in terms of (a) relaxation of  $\text{REE}^{3+}/\text{Na}^+$  and cation ( $\text{Ca}^{2+}$ )-vacancy dipoles, (b) a strong and persistent ion-jump relaxation effect which dominates in the annealed samples, and (c) dipole-clustering phenomena.

## ACKNOWLEDGMENTS

Supply of the XRD spectra and Rietvelt analysis results by Professor Dr. M. Calamiotou and A. Gantis (Physics Department, Athens University) is gratefully acknowledged. The authors are also indebted to Dr. V. Perdikatsis (Institute of Geology and Mineral Exploration, Athens) for the DTA, and Dr. A. Karidas and Dr. Th. Paradellis (Laboratory for Mineral Analysis, Institute of Nuclear Physics, NRCPS "Demokritos") for the XRF analysis.

- <sup>1</sup>W. A. Deer, R. A. Howie, and J. Zussman, *An Introduction to the Rock forming Minerals* (Longman, Green, New York, 1985), pp. 504–509.
- <sup>2</sup>R. W. G. Wyckoff, *Crystal Structures*, 2nd ed. (Interscience, New York, 1965), Vol. III, p. 228.
- <sup>3</sup>D. W. Davis, E. S. Schandl, and H. A. Wastneys, *Contrib. Mineral. Petrol.* **114**, 427 (1994).
- <sup>4</sup>K. De Groot, *Biomaterials* **1**, 47 (1980).
- <sup>5</sup>D. McConnell, *Apatite, Its Crystal Chemistry, Mineralogy Utilization and Geologic and Biologic Occurrences*, Applied Mineralogy Vol. 5 (Springer, Wien, 1973).
- <sup>6</sup>M. E. Fleet and Y. Pan, *Eur. J. Mineral.* **7**, 591 (1995).
- <sup>7</sup>H. S. Yoon and R. E. Newnham, *Am. Mineral.* **54**, 1193 (1969).
- <sup>8</sup>R. W. Warren, *Phys. Rev. B* **2**, 4383 (1970).
- <sup>9</sup>P. E. Mackie, J. C. Elliott, and R. A. Young, *Acta Crystallogr., Sect. B: Struct. Crystallogr. Cryst. Chem.* **28**, 1840 (1972).
- <sup>10</sup>M. H. Battey, *Mineralogy* (Longman, Green, New York, 1981), p. 227.
- <sup>11</sup>R. A. Young and J. C. Elliot, *Arch. Oral Biol.* **11**, 699 (1966) [cf. *Trans. NY Acad. Sci.* **29**, 949 (1966)].
- <sup>12</sup>N. Hitmi, C. Lacabanne, and R. A. Young, *J. Phys. Chem. Solids* **45**, 701 (1984).
- <sup>13</sup>N. Hitmi, C. Lacabanne, G. Bonel, and R. A. Young, *J. Phys. Chem. Solids* **47**, 507 (1986).
- <sup>14</sup>N. Hitmi, C. Lacabanne, and R. A. Young, *J. Phys. Chem. Solids* **47**, 533 (1986).
- <sup>15</sup>I. M. Kalogeras and A. Vassilikou-Dova, *Cryst. Res. Technol.* **31**, 693 (1996).
- <sup>16</sup>N. Hitmi, Thésé, Université Paul Sabatier, Toulouse, 1983.
- <sup>17</sup>N. Hitmi, C. Lacabanne, and R. A. Young, *J. Phys. Chem. Solids* **49**, 541 (1988).
- <sup>18</sup>N. Hitmi, D. Chatain, C. Lacabanne, J. Dugas, J. C. Trombe, C. Rey, and G. Montel, *Solid State Commun.* **33**, 1003 (1980).
- <sup>19</sup>E. J. Young, A. T. Myers, E. L. Munson, and N. M. Conklin, *U.S. Geol. Survey Prof. Paper* **650**, D84 (1969).
- <sup>20</sup>C. Bucci and R. Fieschi, *Phys. Rev. Lett.* **12**, 16 (1964); C. Bucci, R. Fieschi, G. Guidi, *Phys. Rev. B* **148**, 816 (1966).
- <sup>21</sup>I. M. Kalogeras and A. Vassilikou-Dova, *Defect and Diffusion Forum* **164**, 1 (1998).
- <sup>22</sup>J. Vanderschueren and J. Gasiot, in *Thermally Stimulated Relaxation in Solids in Topics in Applied Physics*, edited by G. M. Braunlich (Springer, Berlin, 1979), Vol. 33, p. 81.
- <sup>23</sup>S. A. Howard, Department of Ceramic Engineering, University of Missouri-Rolla, MO 65401.
- <sup>24</sup>A. Vassilikou-Dova, Ph.D. thesis, University of Athens, 1985.
- <sup>25</sup>*Point Defect in Solids, General and Ionic Crystals*, edited by J. H. Crawford, Jr. and L. M. Q. Slifkin (Plenum, New York, 1972), Vol. 1, pp. 151–200.
- <sup>26</sup>E. O. Rausch, thesis, Georgia Institute of Technology, 1976.
- <sup>27</sup>R. A. Young, W. van der Lugt, and J. C. Elliot, *Nature (London)* **223**, 729 (1969).
- <sup>28</sup>J. G. Ronsbo, *Am. Mineral.* **74**, 896 (1989).
- <sup>29</sup>J. M. Hughes, M. Cameron, and A. N. Mariano, *Am. Mineral.* **76**, 1165 (1991).
- <sup>30</sup>P. L. Roeder, D. MacArthur, X. P. Ma, and G. R. Palmer, *Am. Mineral.* **72**, 801 (1987).
- <sup>31</sup>I. Roelandts, *Chem. Geol.* **67**, 171 (1988).
- <sup>32</sup>*Handbook of Physical Constants*, edited by S. P. Clark, Jr. (Geol. Soc. Amer. Mem., New York, 1966), Vol. 97, p. 566.
- <sup>33</sup>P. P. Phakey and J. R. Leonard, *J. Appl. Crystallogr.* **3**, 38 (1970).
- <sup>34</sup>D. M. Burt, *Rev. Mineral.* **21**, 259 (1989).
- <sup>35</sup>E. J. Young and E. L. Munson, *Am. Mineral.* **51**, 1476 (1966).
- <sup>36</sup>R. A. Young, K. Sudarsanan, and P. E. Mackie, *Bull. Soc. Chim. Francies (No Spécial)* (1968), p. 1760.